Journal of Materials Chemistry A

Accepted Manuscript

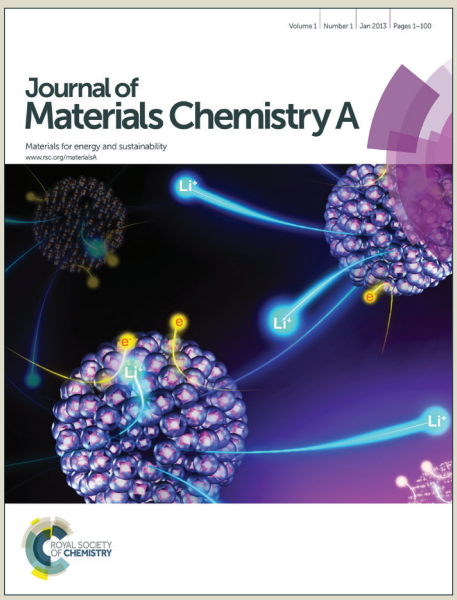

ROYAL SOCIETY OF CHEMISTRY

www.rsc.org/materialsA

Journal Name

RSCPublishing

ARTICLE

Combinatorial optimization of spinel $Co_{3-x}M_xO_4$ M = (Al, Ga, In) alloyed thin films prepared by ink jet printing: photoelectrochemical, optical, and structural properties†

Cite this: DOI: 10.1039/x0xx00000x

Received ooth January 2012,
Accepted ooth January 2012

DOI: 10.1039/x0xx00000x

www.rsc.org/

P. F. Newhouse[a,b] and B. A. Parkinson[a*]

The photoelectrochemical, optical, and structural properties of semiconducting spinel oxide solid solutions and mixed phase thin films of $Co_{3-x}M_xO_4$ [M = (Al, Ga, In)] are investigated as a function the Al:Ga:In alloying ratio and the total Co substitution amount, x. The highest photocurrent, and improved dark currents relative to unalloyed Co_3O_4 films, were measured from films with Al:Ga:In ratios of ~1.5:1:1.9 at x = 0.4. Glancing angle XRD reveals a lattice expansion upon alloying when $x \geq 0.6$ along with a general disordering of the crystal structure that appears to correlate with the In mole fraction since In has limited solubility in the spinel structure. However, an optimal balance of properties may be achieved, within the In solubility range, by the combined effects of the group IIIB elements resulting in higher cathodic photocurrents relative to unalloyed Co_3O_4 even though the optical absorption of the alloyed compositions is systematically reduced and blue shifted. SEM analysis reveals clear changes in film morphology exhibiting a smoother surface when $x \geq 0.6$. This work demonstrates that combinatorial band engineering can help optimize the photoelectrochemical performance of Co_3O_4 by offsetting losses in optical absorption via improved carrier transport.

[a] University of Wyoming Department of Chemistry, Laramie, WY 82071
[b] Present address: Joint Center for Artificial Photosynthesis, California Institute of Technology, Pasadena, CA 91125
*Author to whom correspondence should be addressed, bparkin1@uwyo.edu

† Electronic Supplementary Information (ESI) available: powder x-ray diffraction data. See DOI: 10.1039/x0xx00000x

Introduction

The storage of solar energy is perhaps the largest obstacle for the large-scale adoption of this renewable resource[1]. An ideal way to store solar energy for nighttime and transportation use is by directly splitting water with sunlight to produce hydrogen fuel. Connecting conventional photovoltaic cells to a commercial electrolyzer would be one method for accomplishing this goal, however these are two expensive technologies. A more cost effective system may be to immerse the semiconductor photoelectrodes directly into the electrolyte and use the semiconductor electrolyte interface to separate the photogenerated charges to perform the photoelectrolysis in one device[2]. The problem with this approach is that semiconducting materials that are efficient, inexpensive and stable in an electrolyte solution for long periods of time remain unknown. Our group has argued that metal oxide semiconducting electrodes would be most suited for this application[3]. In order to quickly produce and screen multicomponent oxides for their ability to photooxidize or photoreduce water, we developed a simple and effective high throughput combinatorial technique that uses ink jet printing of metal oxide precursors onto conductive glass substrates to produce libraries of multicomponent oxides to screen for photoelectrolysis activity[4]. Using this protocol, one of the first discoveries of a semiconductor exhibiting a band gap suitable for utilization of the solar spectrum (~1.0–2.0 eV), was a cobalt-rich $Co_{1-x-y}Fe_xAl_yO_4$ spinel[5]. Although this material has yet to exhibit high quantum yields for the production and collection of photogenerated charges, it appears to be quite stable and has a band gap of ~1.5 eV, making it potentially useful in a real device especially with appropriate nanostructuring of the device to mitigate the generally short carrier diffusion lengths of many metal oxides.

In order to accelerate the discovery of additional promising new oxide semiconductors, we established the Solar Hydrogen Activity research Kit (SHArK) outreach project that recruits

many students to participate in the discovery process[6,7]. Recently[8], a p-type Fe-Cr-Al oxide phase, with the α-Fe_2O_3 structure, was discovered by a SHArK participant and was followed up by our group and found to exhibit a band gap of 1.8 eV with nearly 1V of photovoltage with an optimized composition near $Fe_{0.84}Cr_{1.0}Al_{0.16}O_3$. In addition the Joint Center for Artificial Photosynthesis (JCAP) was established by the Department of Energy to develop a device that photoelectrolyzes water with sunlight and they have committed substantial resources to greatly increasing the throughput of this combinatorial technique to identify new photoelectrode materials[9,10]. Hopefully these efforts will produce dozens of new oxide semiconductor compositions that hold promise for solar water photoelectrolysis. However, if one looks at the history of the development of new thin film photovoltaic materials, it is apparent that many years of research are needed to understand and optimize the materials before they were efficient and understood enough to manufacture commercially feasible devices. It is likely that the same will be true of the new oxide semiconductor materials for photoelectrolysis and that combinatorial techniques will be useful in the optimization and discovery phases. For example, we previously demonstrated that simultaneously adding small amounts of Si, Al and Ti to α-Fe_2O_3 (hematite) photoelectrodes produced synergistic effects in improving the photoresponse of Fe_2O_3, suggesting that the individual added elements do not each act in the same manner[11].

In this contribution we return to the Co_3O_4 spinel system and investigate the effects on the photoresponse and structure by alloying with the group IIIB cations Al, Ga and In. This topic has recently been addressed[12] theoretically by calculating the compositions needed for optimally balanced photoelectrochemical properties (e.g. band gap, carrier transport) induced by the combinatorial effects of these cations in Co_3O_4. Previous experimental work in this area focused on discretely treating each of the group IIIB cations in Co_3O_4 (e.g. $CoAl_2O_4$, $CoGa_2O_4$, $CoIn_2O_4$) and hence did not observe the favorable effects induced by alloying In, which can only be incorporated in limited amounts due to lattice strain[13].

Experimental

Pilkington Tec-15 SnO_2:F (FTO) glass was obtained from Hartford Glass Co. and washed thoroughly with a sponge in flowing warm water with Alconox solution followed by rinsing with 18 MΩ water and N_2 blow drying. The cleaned, dried surface is then immediately sprayed with methanol and again blown dry and placed on the printer platen to equilibrate at the set print temperature for 2-5 minutes at 60 C. The methanol is used to increase the hydrophobicity of the FTO surface just prior to printing even though most of it desorbs. This reduces the ink wetting slightly and helps maintain the desired feature shapes. 0.2M nitrate salt solutions of Co [$Co(NO_3)_2 \bullet 6H_2O$, Strem], Al [$Al(NO_3)_3 \bullet 9H_2O$, Sigma-Aldrich], Ga [$Ga(NO_3)_3 \bullet xH_2O$, Sigma-Aldrich] and In [$In(NO_3)_3 \bullet xH_2O$, Sigma-Aldrich] were prepared using an aqueous-based solvent solution containing 35% diethelynene glycol and 1% diethelyene glycol monobutyl ether. This ink base solvent exhibits sufficient solubility for many nitrate salts and meets viscosity and surface tension requirements for good droplet formation. The 0.2M single element solutions were used for gradient and discrete composition printing in which the lower concentrations enabled good precursor mixing of the printed layers prior to pyrolysis. To examine the effect of total Co substitution by the optimal Al-Ga-In mixture (hereafter referred to as "group IIIB" and "B^{opt}"), four element solutions of $Co_{3-x}B^{opt}_x$ [x = 0, 0.2...0.8; 0.35M total] were prepared and injected into individual printheads. All solutions were sonicated in a Misonix XL-2000 stick sonicator at 3W power for 10-20 minutes prior to filtered syringe injection into the printhead. Many metal nitrate salts exhibit varying degrees of water content and this can be a source of significant error when determining feature stoichiometries if an accurate formula weight is difficult to determine. For this reason thermal gravimetric analysis (TA Instruments Q600) was performed on hydroscopic precursor salts like $In(NO_3)_3$ and $Ga(NO_3)_3$ so that accurate molarity solutions could be prepared or determined if not known initially. The drier Al and Co nitrate salts with stated hydration content were used as received. The cleanliness and preparation of the FTO surface, ink concentration, substrate temperature, and the water/glycol ratio of the ink solvent all impact the precursor mixing and surface wetting of the inks, which can greatly impact the morphology of the oxide films. Often compositional "hotspots" are misinterpreted because the observed high photocurrent is driven primarily by surface area and/or thickness rather than composition. To compare samples of different composition they should have equivalent morphologies and thicknesses to first order.

A Fuji-Dimatix DMP-2810 single channel peizoelectric ink jet printer was used to print all patterns at a jetting frequency of 5 kHz. The jetting status of the 16 nozzles of a given printhead must be monitored diligently because the nozzles can dry out, become clogged or otherwise exhibit altered drop trajectories and/or velocities, leading to inaccurate total drop counts and erroneous stoichiometry assignments. For this reason, the jetting status of each of the nozzles on a given printhead is monitored using a camera just prior to printing, and cleaning cycles consisting of a positive pressure purge and nozzle wipe are run frequently to help ensure reliability. The total drop count within a given feature is used with the average volume of each drop (typically 7 pL, measured gravimetrically) and the ink concentration to calculate the stoichiometry of a given feature. For exploration of large compositional spaces, triangle-shaped overprint and vertex gradient templates were created in Adobe Photoshop at drop resolutions chosen to span specific stoichiometric ranges of interest. Discrete composition print patterns consisting of an 8 x 8 grid were created in the printer software platform and were used to determine the photoactivty of specific stoichiometries near a composition region of interest rather than investigate large compositional spaces. Additional working details of this ink jet printer and the quantification of the printed drops can be found in earlier work[4,5]. Following

printing, films were immediately sintered in air at 625 °C for 90 minutes (10°C/min ramp) using a Thermo Scientific Lindberg Blue box furnace. We found no degradation in the FTO conductivity under such conditions.

The photocurrent measurements of Figures 1-3 were performed in two electrode configuration at zero applied bias (FTO working electrode, shorted counter & reference electrodes) using a JMDL 532 nm laser beam (~30 mW, ~1 mm beam diameter) chopped at 31 Hz. The samples were oriented for backside illumination and immersed in a glass cell containing 0.1M unpurged NaOH with a 4" x 4" planar graphite counter electrode (CE) positioned directly behind the working electrode (WE). In this geometry, each illuminated feature on the WE is always equidistant from the CE as the laser beam is rastered, a detail we found to be critical when comparing the relative photocurrent intensity from features at different (*x,y*) locations on the WE. We found that other WE/CE geometries using a smaller or different shape CE (e.g. small graphite rods) induced a measurement artifact in which samples on the WE spatially closer to the CE exhibited spuriously higher photocurrent than samples further away. The use of unpurged NaOH electrolyte generally implies that the photocurrent is the result of direct water oxidation for photoanodes and oxygen reduction for photocathodes. We maintain this assumption in the present work and add that these materials are p-type. The WE was connected to a Princeton Applied Research 174A potentiostat coupled to a Stanford Research Systems DSP 810 digital lock-in amplifier which performed an auto phase adjustment prior to each measurement to optimize the photocurrent signal. A pair of orthogonal mirrors (Eye Magic Inc.) was used with an in-house data collection routine to raster the beam over the WE and record the data. For photocurrent-voltage measurements, ~1cm x 1cm films on FTO were contacted using Cu wire and graphite paste and o-ring sealed inside a cell containing unpurged 0.1M NaOH. The film/FTO working electrode, a Ag/AgCl reference electrode, and a Pt wire counter electrode were connected to an Ivium CompactStat potentiostat which swept the voltage (0.02 V/s) and recorded the current as a JMDL 532 nm laser irradiated the working electrodes from the backside (~6 mm expanded beam diameter, 74 mW incident power). Image processing was performed the using IGOR software suite.

SEM images were obtained using an FEI Quanta 450 scanning electron microscope using a 70° sample mount, enabling both cross sectional and topographic images to be obtained simultaneously. The images were obtained from a single substrate containing multiple films of approximately equal thickness and uniform coverage. The films were scribed through their centers from the backside and cleaved. Glancing angle x-ray diffraction measurements (Cu Kα_1, 0.8° incidence, 0.3-0.4°/min, step 0.02°, 2 mm exit slit) were obtained using a Rigaku SmartLab diffractometer with a coupled diffracted beam monochrometer and scintillation counter detector. Each sample was aligned vertically using the tool software routine and the smallest exit slit allowable was used to achieve high angular resolution. The samples were of approximately even thickness, coverage, and area such that peak intensity changes can be interpreted semi-quantitatively. Optical absorption measurements were obtained using a Perkin Elmer Lambda 9000 spectrometer with a blank FTO substrate serving as a reference.

Results and Discussion

Combinatorial Optimization

A false color photocurrent image of a combinatorial library showing the dependence of photocurrent on composition for group IIIB-containing spinel alloys and mixed phases of $Co_{3-x}(Al,Ga,In)_xO_4$ is shown in Fig. 1A. The printing template is shown in Fig. 1B consisting of uniform Co layers interspersed with gradient Al, Ga, and In layers. The total group IIIB content is $x \sim 1$ at any location within the library, and at a given vertex the nearly pure, unalloyed compound is present, e.g. Co_2AlO_4 or Co_2GaO_4. However, at or near the In vertex Co_2InO_4 is probably not present since the spinel crystal structure cannot tolerate the strain induced by the large In^{3+} cation at such high concentrations (effective ionic radius, r^{ion} = 0.8 Å, octahedral coordination[16]). In contrast, we have observed that Al^{3+} (r^{ion} = 0.54 Å) and Ga^{3+} (r^{ion} = 0.62 Å) may be alloyed feely into $Co_{3-x}(Al,Ga)_xO_4$ for $x \leq 2$ (see supplemental information). Indeed, the Al and/or Ga containing Co_3O_4 spinels are well known[14,15] and closer in size to Co^{3+} (r^{ion} = 0.55 Å). Away from the In vertex, crystalline In-containing spinel compositions may exist as the strain from the large In^{3+} is reduced. The photocurrent image shows that In-rich compositions exhibit the highest photocurrent and that the alloyed phases all show higher photocurrents than the pure Co_3O_4 control features (appearing as small rectangles at the bottom). The photocurrent in the hotspot is about a factor of four higher than analogous regions near the Al and Ga verticies, and a factor of about 5.5 higher than the pure Co_3O_4 control features. The vertex regions of mostly pure Co_2AlO_4 and Co_2GaO_4 exhibit weaker photocurrents relative to the In-rich hotspots and may be due to differences in absorption coefficient, charge carrier mobility, or space charge layer thickness in that part of the film. Indeed, recent theoretical work revealed that Al alloying in $Co_{3-x}Al_xO_4$ does not significantly alter the band edge electronic structure because the Al 3*s* states lie at too low binding energy to effectively hybridize the Co *d*-derived band edges[12]. However the incorporation of Ga and/or In introduces larger, higher binding energy Ga 4*s* and In 5*s* atomic states which do hybridize the conduction band minimum (CBM), imparting strong *s* orbital character with a downward, parabolic curvature. This has the effect of lowering the band gap energy since the position of valence band maximum (VBM) is predicted to remain largely unchanged as a function of alloy composition. The more strongly dispersed bands result lower carrier effective mass (e.g. improved carrier mobility) and stronger optical absorption[12]. In essence, the polaron-dominated conductivity of Co_3O_4 gives way to more band-like conductivity with incorporation of Ga and In but not Al.

Journal Name

RSCPublishing

ARTICLE

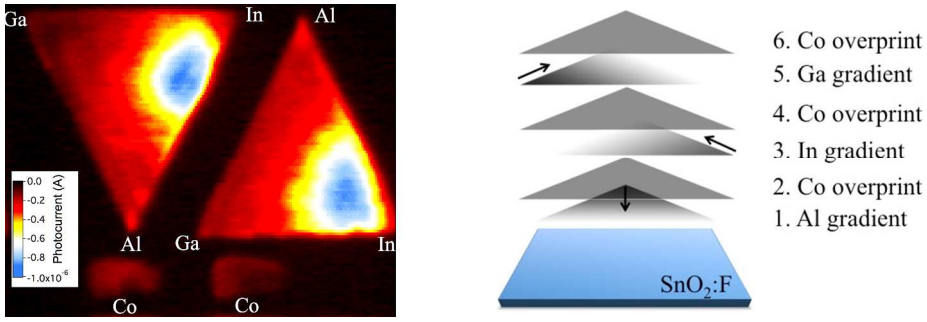

Fig. 1 (A) False color photocurrent image of the feature described by the printing template in (B) and pure Co_3O_4 control films on bottom (redundant and nested features are printed for indication of reproducibility). At a given vertex essentially the single element group IIIB-Co_3O_4 alloy is present, e.g. Co_2AlO_4 and Co_2GaO_4. In-rich phases exhibit the highest photocurrent, and alloyed phases exhibit higher photocurrent than pure Co_3O_4 on bottom. (B) Printing template and printing order for triangle features in (A). Gradient patterns of Al, Ga, and In are printed on overprints of only Co in the order shown. The staggered print sequence (e.g. Al-Co-In-Co, etc.) ensures good mixing of the precursor inks and determines the total alloy thickness.

On this basis one could expect Co_2GaO_4 and Ga-rich compositions, with their lower band gap and better transport properties to exhibit improved relative photocurrent but our finding is consistent with previous work on pure $CoGa_2O_4$ showing poor PEC performance attributable to poor electron transfer kinetics[13]. However, from our discrete stoichiometry libraries presented below, we find that Ga is an essential component of the optimal alloy composition and we hypothesize it could play a role in increasing the In solubility in the spinel lattice. In the In-rich composition region, the film is darker with a higher optical absorption than the Al and Ga-rich regions, indicative of a lower bandgap that is more favorable for solar energy conversion.

To more quantitatively determine the composition of the highest photocurrent region from Fig. 1, a plate containing an array of samples of discrete compositions designed to "zoom-in" on the hot zone was printed and laser scanned. A false color photocurrent intensity plot of this plate and the printing template are shown in Fig 2. The aluminum ink was printed in double rows of equal concentrations, gallium as double columns, and indium in an "S" pattern within groups of four samples at intersecting double rows and double columns. The relative stoichiometry of each row, column, and group of four features is labeled on the template. Similar to the printing template in Fig. 1, the plate from Fig. 2 was prepared by staggering the print sequence of the Co and group IIIB inks to ensure good precursor mixing. The Co precursor is printed uniformly so that each feature on the plate has the same Co content and only the group IIIB content is varied (the uniform printing of Co is omitted from the template for clarity). The relative Co stoichiometry for each sample on the plate is 14.2, corresponding to $Co_{2.3}B^{total}{}_{0.7}O_4$. The template contains a double column with no gallium as a control in order to determine if any gallium was required since earlier experiments indicated that only small amounts of gallium were needed to achieve high photocurrents. The samples in the Ga 0 column all exhibited lower photocurrents compared to samples containing Ga. Therefore, it is clear that a comparatively small mole fraction of Ga is an essential component of an optimized group IIIB stoichiometry. The sample exhibiting the strongest photocurrent in Fig. 2A is indicated by a white box, corresponding to a stoichiometry of Al:Ga:In = 1.5:1:1.9. The complete composition of this feature is approximately $Co_{2.3}Al_{0.24}Ga_{0.16}In_{0.3}O_4$. The total Co content in this library is slightly higher compared to the features in Fig. 1, but the optimal alloy composition probably does not vary strongly when x is small in $Co_{3-x}B_xO_4$, e.g. $x \leq 1$. It is possible that the role of Ga may be structural rather than electrochemical: the intermediate-sized Ga could serve as a

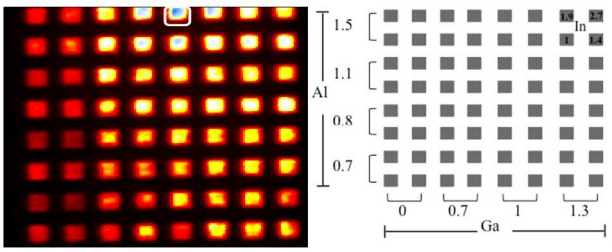

Fig. 2 False color photocurrent image (A) and printing template (B) for a discrete composition "zoom-in" grid designed to span the composition region of the hotspot of Fig. 1. The printing sequence includes overprints of a pure Co grid (not shown) and lists the group IIIB stoichiometry of each sample in the grid, organized by double rows of Al, double columns of Ga, and "S"-pattern groupings of In at the intersection of row and column pairs. The relative Co content of each feature in the grid is 14.2. The most intense photocurrent was measured from the sample enclosed by the white box in (A), that has a group IIIB stoichiometry ratio of 1.5:1:1.9 Al:Ga:In, or $Co_{2.3}Al_{0.24}Ga_{0.16}In_{0.3}O_4$

size "go-between" for substitution of the small Al and Co ions by the much larger In ion, but a balance must be struck between maximum In solubility and crystallinity, both of which were found to be characteristics of the best performing materials.

Optical Absorption from Alloyed Films

The photocurrent data in Figs 1 and 2 revealed the optimal alloying ratio for the case of $x \sim 1$ and $x \sim 0.7$ in $Co_{3-x}B_xO_4$. We turn now to the question of how much Co should be replaced in $Co_{3-x}B^{opt}{}_x$ to achieve the highest photocurrent and the corresponding optical absorption from these films. From previous studies[5] it is known that the highest photocurrent for Co_3O_4-based oxides comes from alloyed, yet still Co-rich phases, as in $Co_{2.5}Fe_{0.3}Al_{0.18}O_4$. In the top pane of Fig. 3 a false color photocurrent image from several $Co_{3-x}B^{opt}{}_x$ features with x = [0, 0.2..0.8] is shown along with a photograph of the films. The data show that the highest photocurrent occurs when x = 0.4 and that even relatively dilute alloying (e.g. x = 0.2) improves the photocurrent relative to pure Co_3O_4. However, at higher alloy content (e.g. x = 0.6, 0.8) the photocurrent diminishes and the films become more transparent. It is possible that this reduction in photocurrent coincides with reduced electrical conductivity as the alloying elements compensate too many of the native, charge generating defects. Concurrently, the structure becomes more disordered as the total In mole fraction is increased, leading to lower photocurrent. Optically, a decrease in the optical absorption of the films might be expected if one considers that the oxide band gaps of the alloying elements, e.g. Al_2O_3, Ga_2O_3, (E_g >> 3 eV) are significantly larger than pure Co_3O_4 (E_g ~ 1.4 eV). The visible-NIR optical absorption data from this series of films is presented in the lower pane of Fig 3 (a grating change discontinuity can be observed near 860 nm). Each film exhibits a similar spectral shape with an absorption peak in the range 675-750 nm attributable the Co *d-d* transition. The onset of this absorption feature is systematically blue shifted and the magnitude of the absorption peak reduced as x increases. Interestingly, pure Co_3O_4 exhibits higher absorption in the NIR and a steeper absorption onset yet exhibits the second least photocurrent, indicating that by band engineering the host compound significant improvements can be made for a photoelectrolysis material.

To examine the performance of samples containing both the optimal alloying ratio (e.g. B^{opt}) and total alloy content (e.g. x = 0.4), photocurrent-voltage scans were taken using a pure Co_3O_4 film of equal thickness as a control (Fig. 4). The light and dark reactions are presumed to be oxygen reduction since the electrolyte used for this experiment was unpurged 0.1M NaOH. The optimized film with x = 0.4 exhibits higher cathodic photocurrent as the potential is swept negative of about -0.1V and improved diode characteristics compared to the x = 0 film, that exhibits significant dark current. The dark current improvement from the alloyed sample could be due to the compensation of native defects in Co_3O_4 by the group III ions. Indeed, semi-quantitative two point resistance measurements of the samples in Fig. 3 revealed that the resistance of x = 0.4 film is significantly greater than the

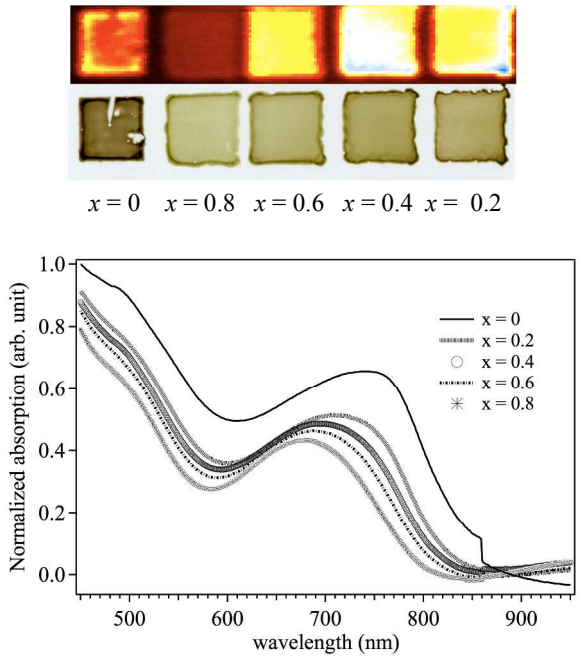

Fig. 3 Optical absorption spectra (lower pane) and false color photocurrent image (upper pane) from the series of $Co_{3-x}B^{opt}{}_xO_4$ films in the photograph. As x increases, the spectra exhibit a systematic blue shift of the primary absorption onset near 850 nm and a reduction of absorption coefficient (a grating change discontinuity is apparent for the x = 0 film). This agrees with inspection of the films, that are darkest for x = 0 and lighten as x increases. The photocurrent image reveals the optimal total Co content in $Co_{3-x}B^{opt}{}_x$ to be x = 0.4

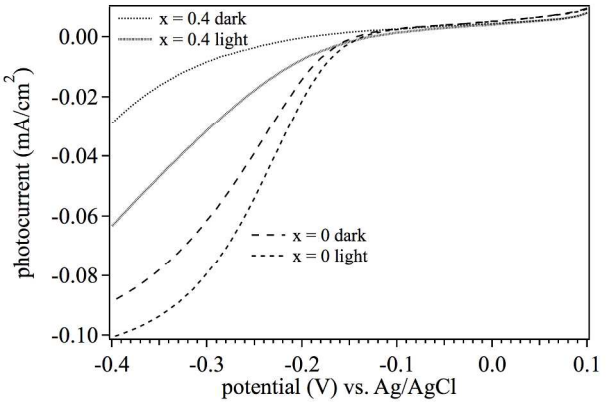

Fig. 4 Dark and illuminated photocurrent-voltage scans in 0.1 M NaOH for a film with near optimal alloying concentration (x = 0.4) and an x = 0 control. The film with x = 0.4 exhibits higher cathodic photocurrent as the potential is swept negative of ~ -0.1V and lower dark current than the control film.

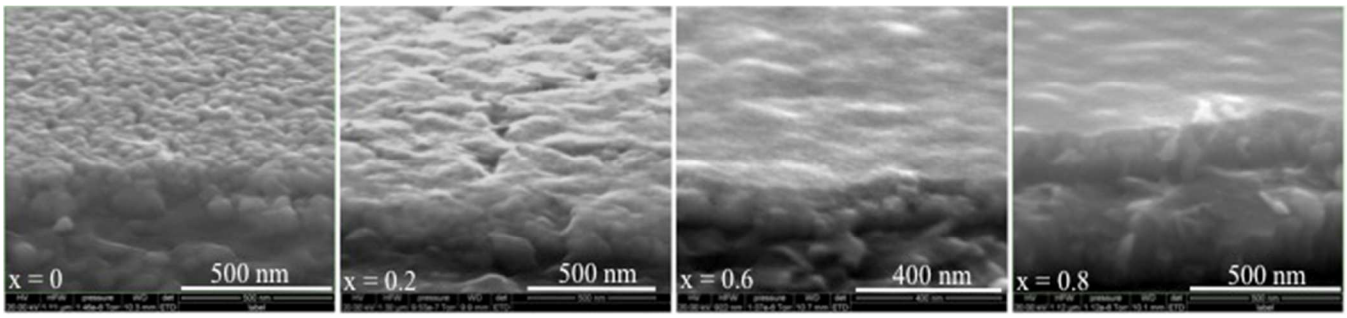

Fig. 5 Cross-sectional/topographical images of (left to right) x = 0, 0.2, 0.6, 0.8 $Co_{3-x}B^{opt}{}_xO_4$ films from Fig 3. The x = 0 surface is nodular and the grains more spherical than the x = 0.2 surface, which appears slightly mud-cracked. Higher alloy content x = 0.6 and 0.8 films appear smoother and more dense, perhaps indicative of more glass-like/disordered structure.

x = 0 sample, and moreover the dark current trace of the x = 0 sample is consistent with a more electrically leaky and/or lower resistance material. The currents are quite small, but the films are thin (~150 nm) and much of the incident light (532 nm, 74 mW backside illumination) is not absorbed.

Film Structure and Morphology

The morphology and film thickness of selected films from Fig. 3 were examined using cross-sectional SEM (Fig. 5). Pure Co_3O_4 films (x = 0) exhibit a nodular surface and cross section with ~70 nm grains. The addition of the group IIIB elements alters the morphology considerably relative to the control, with the x = 0.2 film exhibiting a mud-crack like surface with much more linear and plate-like boundaries. A high quality image of the x = 0.4 film could not be obtained due to sample charging. As the alloy content increases to x = 0.6 and x = 0.8 a surface smoothing trend is observed and small surface bumps can be seen. This observation is in qualitative agreement with the x-ray diffraction patterns from this series of films, which show a general disordering as the content of the alloying element increases. More disordered films may appear smoother and more glassy than the more highly crystalline films. The thicknesses of the films ranged from approximately 140-170 nm, and this range of thicknesses is reasonable considering that the thickness of ink jet printed samples will be strongly dependent on how uniformly the ink wets the substrate, ink drying during heating and volume changes during conversion of the precursor to metal oxide film.

Glancing angle x-ray diffraction patterns from a series of $Co_{3-x}B^{opt}{}_x$ films on FTO from 16-40° 2θ are shown in Fig. 6. This 2θ range contains three spinel diffraction peaks located near 19° (111), 32° (220), and 37° (311, 100% intensity). Substrate FTO reflections are indicated with an asterisk. All the films are polycrystalline with no observable texturing or preferred orientation. Each family of spinel reflections has its peak center shifted to smaller 2θ as the alloy content increases, indicative of the expected lattice expansion (the dashed line serves as a guide to the eye). This is expected since the weighted average ionic radius of the optimal Al-Ga-In alloy is substantially larger than octahedrally coordinated Co^{3+} (0.67 Å vs. 0.55 Å)[16]. Indeed, for high alloy content films with x = 0.8 (red trace), the cation composition is $Co_{2.2}Al_{0.27}Ga_{0.18}In_{0.35}$, equal to 11.5 atom % In and nearing that reported for a high temperature powder preparation of $CoGa_{1.6}In_{0.4}O_4$ (13 atom %)[17]. The reduction of intensity and peak broadening with increasing x is in agreement with our photocurrent and SEM studies which show that as the alloy content goes up (and hence the total In mole fraction) the crystalline grain structure observed at low total alloy content becomes less apparent (e.g. the films appear smoother and more dense in the range above x ~ 0.6 than for the low level alloys below x ~ 0.4) and the photocurrent diminishes. However, as our results show, an optimal ratio and mole fraction of the four cations may be achieved.

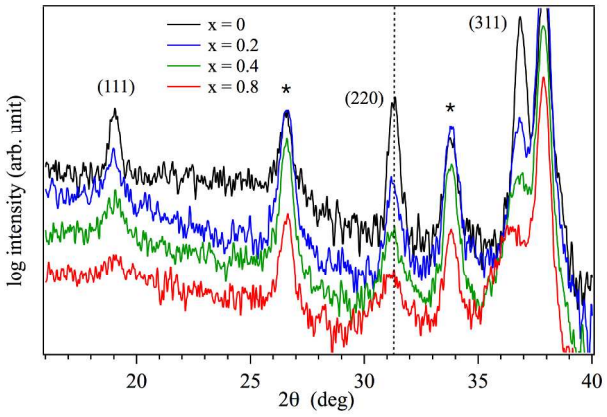

Fig. 6 (color online) Glancing angle x-ray diffraction patterns from a series of $Co_{3-x}B^{opt}{}_x$ films on FTO over 16-40° 2θ□(binomial three point smoothing and offset for clarity). Spinel diffraction peaks are indicated by (*hkl*) listing and FTO substrate peaks are indicated by an asterisk. A slight lattice expansion is measured as x increases (the dashed line is a guide to the eye).

Conclusion

In summary, we have presented the photocurrent optimization of the four cation spinel family $Co_{3-x}M_xO_4$ [M = (Al,Ga,In)] using combinatorial ink jet printing. A greater

than five fold photocurrent enhancement relative to pure Co_3O_4 could be achieved from films simultaneously alloyed with Al, Ga, and In at the ratio 1.5:1:1.9. At this ratio, films with $x = 0.4$ exhibited the highest photocurrent from a series of samples with varying x values. The optical absorption from this series of films was systematically reduced and blue shifted with increasing x relative to Co_3O_4 yet the phototcurrent is enhanced, revealing that improvements in carrier transport properties can offset optical absorption losses. Structurally, the highest photocurrent samples exhibit the crystalline spinel structure, but with increasing In mole fraction the structure becomes disordered and the photocurrent diminishes. The limited solubility of indium in the spinel structure is key to the optimization presented here, with favorable carrier transport properties induced by In 5*s* hybridization of the conduction band in the solubility range and structural disorder above the solubility range. The tolerable limits of In incorporation in Co_3O_4:(Al,Ga,In) depend upon a multitude of synthesis conditions, and a full investigation would be a worthy topic for future study, especially considering the beneficial and understudied effects of In in a crystalline spinel phase.

Nanostructuring, the addition of a specific hydrogen reduction catalysts, and the use of a broadband light sources might further improve the performance of these films, but the merit of the band engineering approach is apparent from these studies. As many simultaneous parameters are at play in such an optimization process, combinatorial techniques will be paramount to moving forward.

Acknowledgements

References

[1] N.S. Lewis and D.G. Nocera, *PNAS*, 2006, **103**, 15729.
[2] F.E. Osterloh and B.A. Parkinson, *Mat. Res. Soc. Bull.*, 2011, **36**, 17.
[3] M. Woodhouse and B.A. Parkinson, *Chem. Soc Rev.*, 2009, **38,** 197.
[4] M. Woodhouse, G.S. Herman, and B.A. Parkinson, *Chem. Mater.*, 2005, **17,** 4318.
[5] M. Woodhouse and B.A. Parkinson, *Chem. Mater.*, 2008 **20,** 2495.
[6] B.A. Parkinson, *Energy Environ. Sci*, 2010, **3**, 509.
[7] P.N. Anunson, G.R. Winkler, J.R. Winkler, B.A. Parkinson and J.D. Schuttlefield, *J. Chem. Ed.* 2013*,* **90***,* 1333.
[8] J.G. Rowley, T.D. Do, D.A. Cleary, and B.A. Parkinson, *Appl. Mater. Interfaces*, 2014, **6**, 9046.
[9] J.M. Gregoire, C. Xiang, S. Mitrovic, X. Liu, M. Marcin, E.W. Cornell, J. Fan, and J. Jin, *J. Electrochem. Soc.* 2013, **160**, F337.
[10] J. Haber, Y. Cai, S. Jung, C. Xiang, S. Mitrovic, J. Jin, A. Bell, and J.M. Gregoire, *Energy Environ. Sci*, 2014, **7**, 682.
[11] J. He and B.A. Parkinson, *ACS Comb. Sci.* 2011, **13,** 399.
[12] C. Feng, W-J. Yin, J. Nie, X. Zu, M.N. Huda, S-H. Wei, M.M. Al-Jassim, J.A. Turner, and Y. Yan, *Appl. Phys. Lett.* 2012, **100,** 023901.
[13] A. Walsh, K-S. Ahn, S. Shet, M.N. Huda, T.G. Deutsch, H. Wang, J.A. Turner, S-H. Wei, Y. Yan, and M.M. Al-Jassim. *Energy Environ. Sci.* 2009, **2,** 774.
[14] The International Centre for Diffraction Data, $CoAl_2O_4$ powder diffraction file 01-082-2246.
[15] The International Centre for Diffraction Data, $CoGa_2O_4$ powder diffraction file 04-013-4218.
[16] R.D. Shannon, *Acta Crystallog., Sect. A*, 1976, **32**, 751.
[17] N. Kimizuka and E. Takayama, *J. Solid State Chem.*, 1984, **53**, 217.